

Multiderivative time integration methods preserving nonlinear functionals via relaxation

Hendrik Ranocha^{*1} and Jochen Schütz^{†2}

¹Institute of Mathematics, Johannes Gutenberg University Mainz, Staudingerweg 9, 55128 Mainz, Germany

²Faculty of Sciences & Data Science Institute, Hasselt University, Agoralaan Gebouw D, BE-3590 Diepenbeek, Belgium

February 7, 2024

We combine the recent relaxation approach with multiderivative Runge-Kutta methods to preserve conservation or dissipation of entropy functionals for ordinary and partial differential equations. Relaxation methods are minor modifications of explicit and implicit schemes, requiring only the solution of a single scalar equation per time step in addition to the baseline scheme. We demonstrate the robustness of the resulting methods for a range of test problems including the 3D compressible Euler equations. In particular, we point out improved error growth rates for certain entropy-conservative problems including nonlinear dispersive wave equations.

Key words. two-derivative methods, multiderivative methods, invariants, conservative systems, dissipative systems, structure-preserving methods

AMS subject classification. 65L06, 65M20, 65M70

1. Introduction

Preserving the correct evolution of a (nonlinear) functional of the solution of a differential equation is an important task in many areas. For ordinary differential equations (ODEs), such a structure-preserving approach is important, e.g., as energy-conserving method for Hamiltonian problems. In general, it falls into the realm of geometric numerical integration [24].

In this article, we concentrate on the preservation of functionals under multiderivative time discretization, including the conservation of invariants as well as dissipative problems. Building on our previous work [56], we use the relaxation approach developed recently in [29, 49, 52]. The first ideas of relaxation go back to [58] and have been refined since then. Originally developed for Runge-Kutta and linear multistep methods, the general theory of [49] can be applied to a wide range of time integration schemes including also deferred correction and ADER methods [2, 19] as well as IMEX schemes [27, 33, 34]. The construction can be extended to multiple invariants [7, 8] and implicit schemes not relying on an exact solution of the equations [35]. Relaxation methods

^{*}ORCID: 0000-0002-3456-2277

[†]ORCID: 0000-0002-6355-9130

have been applied successfully to Hamiltonian problems [48, 70], kinetic equations [32], entropy-stable methods for compressible fluid flows [44, 67], and nonlinear dispersive wave equations [37, 50, 51].

Multiderivative schemes are numerical integration schemes for differential equations that can be traced back to at least [66] in the context of quadrature rules; for ODEs, they have been discussed in [23, 28]. We do not attempt to give a full historic overview, but refer the reader to [63, Section 2.1] for one such thorough overview. In contrast to more established schemes, multiderivative schemes do not only use the ODE's right-hand side, but also temporal derivatives thereof. Recently, these methods have gained renewed interest, as the construction principle allows for very flexible schemes, be it with respect to SSP properties, e.g., [21, 38], efficiency, e.g., [1, 62, 63, 69], stability, e.g., [13, 60, 68] and many others. In this work, we are to our knowledge the first to combine relaxation with the multiderivative approach; results with up to four derivatives will be shown.

In the following Section 2, we briefly review the construction of multiderivative Runge-Kutta methods and the relaxation approach. Section 3 is devoted to the development of appropriate entropy estimates for multiderivative methods applied to non-conservative problems. In Section 4, we discuss stability properties of the relaxed methods. Next, we present numerical experiments in Section 5, ranging from convergence experiments to robustness demonstrations for PDE discretizations as well as qualitative and quantitative improvements via reduced error growth rates. Finally, we summarize the results in Section 6.

2. Basic ideas of multiderivative and relaxation methods

First, we present the basic ideas of multiderivative time integration methods as well as relaxation schemes. Thereafter, we will describe our approach to combine them in Section 3.

2.1. Multi-derivative Runge-Kutta methods

To introduce the methods considered in this paper, we define the initial-value problem

$$u'(t) = f(u(t)), \quad u(0) = u^0 \quad (2.1)$$

for given right-hand side $f: \mathbb{R}^d \rightarrow \mathbb{R}^d$ and initial condition $u^0 \in \mathbb{R}^d$. The basic idea of multiderivative methods is to use not only $u'(t)$, which equals $f(u(t))$, but also higher derivatives such as $u''(t)$, $u'''(t)$, \dots to compute a numerical approximation. All these quantities can be computed using the available data, e.g., $u''(t) = f'(u)f(u)$. (Please note that for the ease of presentation, we from now on refrain from explicitly writing the t -dependency of u in, e.g., terms as $f(u)$.) The most well-known class of schemes using this information are Taylor series methods, which just approximate the solution in one time step by a truncated Taylor series. In this article, we are instead interested in multiderivative methods using additionally the idea to compute multiple internal stages as in Runge-Kutta methods.

Define the higher-order temporal derivatives of $f(u)$ through

$$g^{(1)}(u) := f(u), \quad g^{(2)}(u) := f'(u)f(u), \quad g^{(3)}(u) := f'(u)f'(u)f(u) + f''(u)(f(u), f(u))$$

and so on. Note that for the exact solution to (2.1), there holds $u^{(k)}(t) = g^{(k)}(u)$, where $u^{(k)}(t)$ denotes the k -th temporal derivative of u . Please note that it gets increasingly complex to compute the quantities $g^{(k)}(u)$; we hence limit our numerical computations to four derivatives. With this notation, a multi-derivative Runge-Kutta method with s stages y^i can be written as, e.g., in [28],

$$\begin{aligned} y^i &= u^n + \sum_{k=1}^m \Delta t^k \sum_{j=1}^s a_{ij}^{(k)} g^{(k)}(y^j), \\ u^{n+1} &= u^n + \sum_{k=1}^m \Delta t^k \sum_{i=1}^s b_i^{(k)} g^{(k)}(y^i). \end{aligned} \quad (2.2)$$

m is the number of derivatives taken into account (there holds $m = 1$ for the classical Runge-Kutta schemes); the coefficients $a_{ij}^{(k)}$ and $b_i^{(k)}$ can as usual be represented through an extended Butcher tableau

$$\begin{array}{c|c|c|c|c} c & A^{(1)} & A^{(2)} & \dots & A^{(m)} \\ \hline & b^{(1)} & b^{(2)} & \dots & b^{(m)} \end{array} \quad (2.3)$$

where $A^{(k)} = (a_{ij}^{(k)})_{ij} \in \mathbb{R}^{s \times s}$, $b^{(k)} = (b_i^{(k)})_i \in \mathbb{R}^s$, and $c = (c_i)_i \in \mathbb{R}^s$ with $c_i = \sum_{j=1}^s a_{ij}^{(1)}$.

In this work, we will use the following classes of schemes:

- The third-, fourth-, and fifth-order explicit schemes of Chan and Tsai [13]. They belong to the class of two-derivative schemes; only their order p and number of stages s differ. They are referred to as CT(p , s). For convenience, the Butcher tableaux have been reported in Sec. A.1. Note that CT(4, 2) has the same stability region as the original fourth-order Runge-Kutta method, but requires only one $g^{(1)}$ and two $g^{(2)}$ evaluations instead of four $g^{(1)}$ evaluations.
- The explicit three-derivative schemes of order $p = 5$ and $p = 7$, respectively, of Turaci and Öziş [65]. They are referred to as TO(p , s), with s denoting again the number of stages. Butcher tableaux are reported in Sec. A.2.
- The third- and fourth-order two-derivative SSP schemes from Gottlieb and co-workers [21]; they are referred to as SSP-I2DRK3-2s and SSP-I2DRK4-5s, respectively. Also here, the Butcher tableaux can be found in Sec. A.3.
- Some examples of a class of collocation-based, fully implicit schemes, called Hermite-Birkhoff methods. We refer to these methods as HB- Im DRK p - ss , where again m denotes the number of derivatives, p denotes the order and s the number of stages. Butcher tableaux of HB-I2DRK4-2s and HB-I2DRK6-3s can be found in Tables 1 and 2, respectively (set $\theta = 1$); all the other methods can be generated through a Matlab code in our reproducibility repository [55]. These methods are defined by prescribing the coefficients c through an equidistant spacing of $[0, 1]$, i.e., $c_i := \frac{i-1}{s-1}$, $1 \leq i \leq s$. Then, a standard collocation approach is performed, with the exception that m derivatives of u are taken into account rather than only one. For more information, consult [25] (for $m = 1$) and (3.7). An exception to this construction principle is the HB-I2DRK3-2s method that uses Hermite-Birkhoff interpolation on $c = (0, 1)^T$ with one derivative at the left, and two derivatives at the right point. In two-point notation, it can be written as

$$u^{n+1} = u^n + \frac{\Delta t}{3} \left(g^{(1)}(u^n) + 2g^{(1)}(u^{n+1}) \right) - \frac{\Delta t^2}{6} g^{(2)}(u^{n+1});$$

it is both A - and L -stable.

2.2. Relaxation methods

Next, we describe relaxation methods following the general theory of [49], specialized to one-step methods. Consider a one-step method computing a numerical solution u^{n+1} at time $t^{n+1} = t^n + \Delta t$ from the previous step u^n . Assume that there is a functional η of the solution u of (2.1) that should be preserved. In many cases, the functional η can be interpreted as an “energy” or “entropy” of the solution. In this paper, we will usually call η an entropy. Some important cases are invariants satisfying $\frac{d}{dt}\eta(u(t)) = 0$ and dissipative problems where $\frac{d}{dt}\eta(u(t)) \leq 0$.

The basic idea of relaxation methods is to post-process a baseline solution and continue the numerical integration using

$$u_\gamma^{n+1} = u^n + \gamma \left(u^{n+1} - u^n \right) \quad (2.4)$$

as the numerical approximation at time

$$t_\gamma^{n+1} = t^n + \gamma (t^{n+1} - t^n) \quad (2.5)$$

instead of the baseline solution u^{n+1} at time t^{n+1} . The relaxation parameter γ is computed by solving the scalar root finding problem

$$\eta(u_\gamma^{n+1}) = \eta(u^n) + \gamma(\eta^{\text{new}} - \eta(u^n)), \quad (2.6)$$

where η^{new} is an estimate of the entropy at t^{n+1} , i.e., $\eta^{\text{new}} \approx \eta(u(t^{n+1}))$. For entropy-conservative problems, we use $\eta^{\text{new}} = \eta(u^n)$, ensuring discrete entropy conservation of the form $\eta(u_\gamma^{n+1}) = \eta(u^n)$. For dissipative problems, we require $\eta^{\text{new}} \leq \eta(u^n)$, resulting in discrete entropy dissipation of the form $\eta(u_\gamma^{n+1}) \leq \eta(u^n)$. We will describe how to obtain such estimates for multiderivative methods in the following Section 3.

Remark 2.1. If the entropy is given by an inner product norm, i.e., $\eta(u) = \|u\|^2 = \langle u, u \rangle$, the relaxation parameter can be computed explicitly [29, 49]. For a conservative problem,

$$\gamma = -2 \frac{\langle u^n, u^{n+1} - u^n \rangle}{\|u^{n+1} - u^n\|^2}, \quad (2.7)$$

while a general (e.g., dissipative) problem yields

$$\gamma = \frac{\eta^{\text{new}} - \eta(u^n) - 2\langle u^n, u^{n+1} - u^n \rangle}{\|u^{n+1} - u^n\|^2}. \quad (2.8)$$

If general entropies are considered, one has to rely on *scalar* root-finding algorithms such as Newton-Raphson or bisection. \triangleleft

The theory of [49] yields the following result:

Theorem 2.2. Consider the relaxation procedure described above for a one-step method of order $p \geq 2$ with exact value at time t^n , i.e., $u^{n+1} = u(t^{n+1}) + \mathcal{O}(\Delta t^{p+1})$. If the time step Δt is sufficiently small, $\eta^{\text{new}} = \eta(u(t^{n+1})) + \mathcal{O}(\Delta t^{p+1})$, and

$$\eta'(u^{n+1}) \frac{u^{n+1} - u^n}{\|u^{n+1} - u^n\|} = c\Delta t + \mathcal{O}(\Delta t^2), \quad \text{with } c \neq 0, \quad (2.9)$$

there is a unique solution $\gamma = 1 + \mathcal{O}(\Delta t^{p-1})$ and the relaxation method satisfies $u_\gamma^{n+1} = u(t_\gamma^{n+1}) + \mathcal{O}(\Delta t^{p+1})$.

Thus, the relaxation approach keeps at least the order of accuracy of the baseline method (and can sometimes even lead to superconvergence, e.g., [48]). The non-degeneracy condition (2.9) basically requires that the entropy η is “nonlinear enough”, e.g., strictly convex — since the relaxation approach conserves all linear invariants of the baseline method, in contrast to the orthogonal projection method [24, Section IV.4].

The relaxation approach can be interpreted as a line search along the secant connecting u^n and u^{n+1} . To keep at least the order of accuracy of the baseline method, relaxation methods require adapting the time as well. Otherwise, they result in the incremental direction technique (IDT) of [9], losing an order of accuracy for Runge-Kutta methods [9, 29] and sometimes even more for multistep methods [49].

3. Efficient application of relaxation to multiderivative methods

Multiderivative methods can be combined directly with relaxation methods to conserve an invariant. For more general problems where the entropy is not necessarily conserved, e.g., dissipative

problems, we need to develop an appropriate estimate η^{new} satisfying

$$\eta^{\text{new}} = \eta(u(t^{n+1})) + \mathcal{O}(\Delta t^{p+1}) = \eta(u(t^n)) + \int_{t^n}^{t^{n+1}} \underbrace{(\eta' f)(u(t))}_{=\frac{d}{dt}\eta(u(t))} dt + \mathcal{O}(\Delta t^{p+1}). \quad (3.1)$$

For Runge-Kutta methods, an efficient approach is to use the Runge-Kutta quadrature directly to approximate the integral in (3.1) [29, 52], i.e.,

$$\eta^{\text{new}} = \eta(u^n) + \Delta t \sum_{i=1}^s b_i (\eta' f)(y^i). \quad (3.2)$$

This yields an appropriately dissipative estimate $\eta^{\text{new}} \leq \eta(u^n)$ for dissipative problems if the Runge-Kutta weights b_i are non-negative.

However, we cannot use such an approach with multiderivative methods since we only have information on the first derivative of $\eta \circ u$ in general; even if we know that $\frac{d}{dt}\eta(u(t)) \leq 0$ for a dissipative problem, we typically have no information on the second derivative $\frac{d^2}{dt^2}\eta(u(t))$. Thus, we cannot use the step update formula of a multiderivative method to compute an appropriate estimate η^{new} directly.

3.1. Entropy estimates (not only) for dissipative problems

Here, we follow the approach of [49, Section 3.3], see also [11]. The idea is to approximate the integral in (3.1) by a quadrature rule of order at least p with nodes $\tau_i \in [t^n, t^{n+1}]$ and positive weights $w_i > 0$, resulting in

$$\eta^{\text{new}} = \eta(u^n) + \Delta t \sum_i w_i (\eta' f)(y(\tau_i)), \quad (3.3)$$

where $y(\tau_i)$ are the values of an interpolant y of order at least $p-1$ at the quadrature nodes (i.e., a dense output).

Lemma 3.1. *Assuming that the quadrature weights w_i are positive and that $\eta'(u)f(u) \leq 0$, the expression (3.3) yields a dissipative estimate for dissipative functionals, i.e.,*

$$\eta^{\text{new}} \leq \eta(u^n).$$

In this work, we use Gauss-Lobatto-Legendre quadrature to compute the quadrature weights w_i and points τ_i in (3.3)¹. It remains to determine the values $y(\tau_i)$. Two approaches have been investigated here:

Hermite-Birkhoff interpolation Many multiderivative methods compute already $f(u^n) = g^{(1)}(u^n)$, $g^{(2)}(u^n)$, $f(u^{n+1}) = g^{(1)}(u^{n+1})$, and $g^{(2)}(u^{n+1})$. Thus, we can use them together with u^n and u^{n+1} to compute a quintic Hermite interpolation of the numerical solution. For the special case of four quadrature nodes (which is exact for polynomials of degree ≤ 5), this results in the nodes

$$\tau_1 = t^n, \quad \tau_2 = t^n + \left(\frac{1}{2} - \frac{\sqrt{5}}{10}\right)\Delta t, \quad \tau_3 = t^n + \left(\frac{1}{2} + \frac{\sqrt{5}}{10}\right)\Delta t, \quad \tau_4 = t^n + \Delta t = t^{n+1}, \quad (3.4)$$

¹We could also use a Gauss-Legendre quadrature with one node less to get the same order of accuracy of the quadrature. However, since we often have the values of f at the endpoints, we save an evaluation of the right-hand side f by using Gauss-Lobatto-Legendre nodes.

the weights

$$w_1 = \frac{1}{12}, w_2 = \frac{5}{12}, w_3 = \frac{5}{12}, w_4 = \frac{1}{12}, \quad (3.5)$$

and the interpolants

$$\begin{aligned} y(\tau_1) &= u^n, \\ y(\tau_2) &= \frac{250 + 82\sqrt{5}}{500}u^n + \frac{60 + 16\sqrt{5}}{500}\Delta t f(u^n) + \frac{5 + \sqrt{5}}{500}\Delta t^2 g^{(2)}(u^n) \\ &\quad + \frac{250 - 82\sqrt{5}}{500}u^{n+1} + \frac{-60 + 16\sqrt{5}}{500}\Delta t f(u^{n+1}) + \frac{5 - \sqrt{5}}{500}\Delta t^2 g^{(2)}(u^{n+1}), \\ y(\tau_3) &= \frac{250 - 82\sqrt{5}}{500}u^n + \frac{60 - 16\sqrt{5}}{500}\Delta t f(u^n) + \frac{5 - \sqrt{5}}{500}\Delta t^2 g^{(2)}(u^n) \\ &\quad + \frac{250 + 82\sqrt{5}}{500}u^{n+1} + \frac{-60 - 16\sqrt{5}}{500}\Delta t f(u^{n+1}) + \frac{5 + \sqrt{5}}{500}\Delta t^2 g^{(2)}(u^{n+1}), \\ y(\tau_4) &= u^{n+1}. \end{aligned} \quad (3.6)$$

Continuous Runge-Kutta output The class of Hermite-Birkhoff multiderivative Runge-Kutta methods is collocation-based. In a nutshell — for more information on collocation schemes, see [25] — a collocation scheme is defined as a polynomial y_f of order $p - 1$ that interpolates the derivative $f \equiv g^{(1)}$ at collocation points $t^n + \Delta t c_1, \dots, t^n + \Delta t c_s$. In the case of the Hermite-Birkhoff methods, interpolation has to be understood in the sense of Hermite interpolation. Then, the RK stages and update are defined as

$$y^i = u^n + \int_{t^n}^{t^n + \Delta t c_s} y_f(\tau) d\tau, \quad u^{n+1} = u^n + \int_{t^n}^{t^{n+1}} y_f(\tau) d\tau. \quad (3.7)$$

Using suitable Lagrange basis functions for Hermite interpolation, see [39, Sec. 8.5], these expressions can be written in the form of a linear combination of the $g^{(k)}$, $1 \leq k \leq m$. The same idea can be used to produce continuous output, i.e., produce values $y_\theta \approx u(t^n + \theta \Delta t)$ for $\theta \in [0, 1]$ through

$$y_\theta = u^n + \int_{t^n}^{t^n + \Delta t \theta} y_f(\tau) d\tau.$$

For the fourth-order HB-I2DRK4-2s scheme, this results in the Butcher tableau in Tbl. 1. The Butcher tableau of the sixth-order HB-I2DRK6-3s scheme can be found in the appendix, see. Tbl. 2. More Butcher tableaux, also for more than two derivatives or non-equidistantly spaced collocation points c_s , can be generated with the MATLAB code that can be found in our reproducibility repository [55].

Table 1: Runge-Kutta table of the continuous HB-I2DRK4-2s method. The method is uniformly fourth-order in $0 \leq \theta \leq 1$. As usual, the original Runge-Kutta method is obtained by setting $\theta = 1$.

0	0	0	0	0
1	1/2	1/2	1/12	-1/12
	$\frac{\theta^4}{2} - \theta^3 + \theta$	$-\frac{\theta^3(\theta-2)}{2}$	$\frac{\theta^2(3\theta^2-8\theta+6)}{12}$	$\frac{\theta^3(3\theta-4)}{12}$

Remark 3.2. It can already be mentioned at this point that for the problems we have considered in this work, the difference between using an interpolation-based output or a continuous Runge-Kutta type output is negligible, see Sec. 5. ◀

4. Stability properties

Applying a multiderivative Runge-Kutta method to the scalar linear test problem

$$u'(t) = \lambda u(t), \quad \lambda \in \mathbb{C}, \quad (4.1)$$

results in the iteration

$$u^{n+1} = R(z)u^n, \quad z = \lambda \Delta t, \quad (4.2)$$

where R is the stability function of the method. Analogously to classical Runge-Kutta methods, introducing the relaxation parameter γ in

$$u_\gamma^{n+1} = u^n + \gamma (u^{n+1} - u^n) \quad (4.3)$$

can only increase the size of the stability domain if $\gamma \leq 1$ (cf. Theorem 3.1 of [29]).

Theorem 4.1. *Consider the stability function*

$$R_\gamma(z) = 1 + \gamma (R(z) - 1) \quad (4.4)$$

of a relaxed update. For $0 \leq \gamma_1 \leq \gamma_2$, the stability domain of R_{γ_1} includes the one of R_{γ_2} .

Proof. Let $w := R(z) - 1$. Then, $|R_{\gamma_2}(z)| = |1 + \gamma_2 w| \leq 1$ implies $|R_{\gamma_1}(z)| = |1 + \gamma_1 w| \leq 1$ for $0 \leq \gamma_1 \leq \gamma_2$. \square

Corollary 4.2. *Given $\gamma \in [0, 1]$, the stability domain of the relaxed update*

$$u_\gamma^{n+1} = u^n + \gamma (u^{n+1} - u^n) \quad (4.5)$$

is a superset of the one of the baseline method.

Corollary 4.3. *If the baseline method is A -stable, then its relaxed version is A -stable if $\gamma \leq 1$.*

For $\gamma > 1$, we can expect the stability regions to become smaller. For example, consider the implicit midpoint (Runge-Kutta) method

$$u^{n+1} = u^n + \Delta t f \left(\frac{u^{n+1} + u^n}{2} \right) \quad (4.6)$$

with stability function

$$R(z) = \frac{1 + z/2}{1 - z/2}. \quad (4.7)$$

Then, $z \rightarrow \infty$ yields

$$R_\gamma(z) = 1 + \gamma (R(z) - 1) \rightarrow 1 - 2\gamma. \quad (4.8)$$

Thus, A -stability is lost immediately for $\gamma > 1$. For A -stable methods with a stability domain strictly larger than the left half of the complex plane, we can expect to find an upper bound on the relaxation parameter γ ensuring A -stability. A necessary condition is given in the following theorem.

Theorem 4.4. *For an L -stable method, $\gamma \leq 2$ is necessary for A -stability of the relaxed update.*

Proof. For an L -stable method, $R(\infty) = 0$. Thus, $z \rightarrow \infty$ yields

$$|R_\gamma(z)| = |1 + \gamma (R(z) - 1)| \rightarrow |1 - \gamma|. \quad (4.9)$$

Hence, $\gamma > 2$ implies $|R_\gamma(\infty)| > 1$. \square

The constraint $\gamma \leq 2$ is not prohibitive since $\gamma = 1 + \mathcal{O}(\Delta t^{p-1})$ for a p -th order baseline method.

Lemma 4.5. *The upper bound $\gamma \leq 2$ of Theorem 4.4 is sharp for the implicit Euler method.*

Proof. We have

$$R_\gamma(z) = 1 + \gamma (R(z) - 1) = 1 + \gamma \left(\frac{1}{1-z} - 1 \right) = \frac{1-z + \gamma z}{1-z}. \quad (4.10)$$

For $\gamma = 2$, this becomes

$$R_2(z) = \frac{1+z}{1-z}. \quad (4.11)$$

Up to a scaling of z by a factor of two, this is the stability function of the implicit midpoint method. Monotonicity of the stability domain of the relaxed update (Theorem 4.1) proves the claim. \square

Unfortunately, strict A -stability is lost for the relaxed update with fixed relaxation parameter γ for some methods already for values of γ close to unity. Nevertheless, $A(\alpha)$ -stability is often preserved with reasonable values $\alpha \approx 90^\circ$ as shown in Figures 1 and 2 for some methods.

Remark 4.6. Strictly speaking, L -stability is lost for the relaxed update if $\gamma \neq 1$ since

$$R_\gamma(\infty) = 1 + \gamma (R(\infty) - 1) = 1 - \gamma. \quad (4.12)$$

However, $1 - \gamma = \mathcal{O}(\Delta t^{p-1})$ for a p -th order method. Thus, the deviation is just small and we can still expect to get enough (desired) damping. \triangleleft

Remark 4.7. Strong stability preserving (SSP) methods preserve convex stability properties satisfied by the explicit Euler method [22]. By convexity, relaxed updates of SSP methods are still SSP if $\gamma \in [0, 1]$. There are multiple approaches to extend SSP methods to multidervative schemes, including the recent approach of [21] providing implicit SSP methods without time step constraints. We cannot expect to preserve the SSP property unconditionally for $\gamma > 1$. If relaxation is used to impose an inequality for a convex functional η , it can thus be a reasonable choice to restrict the relaxation parameter γ to $[0, 1]$, i.e., to enable relaxation only if the baseline method is not already η -dissipative. \triangleleft

5. Numerical experiments

We will demonstrate the behavior of the newly developed multidervative relaxation methods in this section. We implemented some two-derivative Runge-Kutta methods in Julia [6]. For them, we use automatic/algorithmic differentiation (AD) with ForwardDiff.jl [57] to compute the second derivative $u'' = g^{(2)}(u) = (f'f)(u)$ in a Jacobian-free manner. We apply discontinuous Galerkin (DG) semidiscretizations of conservation laws implemented in Trixi.jl [54, 59] for simulations of the compressible Euler equations. We discretize the nonlinear dispersive Benjamin-Bona-Mahony equation using methods from SummationByPartsOperators.jl [43], which are based on FFTW.jl [18] for Fourier methods.

Please note that we use a classical method-of-lines approach for the PDE discretizations. Thus, we only discretize the spatial operator of the PDE itself and use AD to compute the second time derivative as $u'' = (f'f)(u)$. An alternative would be to use a Lax-Wendroff approach, requiring the spatial discretization of terms for both the first and the second time derivative simultaneously [4, 31, 63, 64].

The Julia source code to reproduce some numerical experiments is available in our reproducibility repository [55]. The remaining numerical experiments are implemented in MATLAB [36] based on a closed-source inhouse research code developed at Hasselt University using symbolic tools to compute higher derivatives of u .

The numerical experiments are roughly ordered by increasing complexity of the ODE systems. First, we verify the convergence properties for a nonlinear oscillator with quadratic entropy functional and two ODEs with non-quadratic entropies. Afterwards, we consider PDE discretizations:

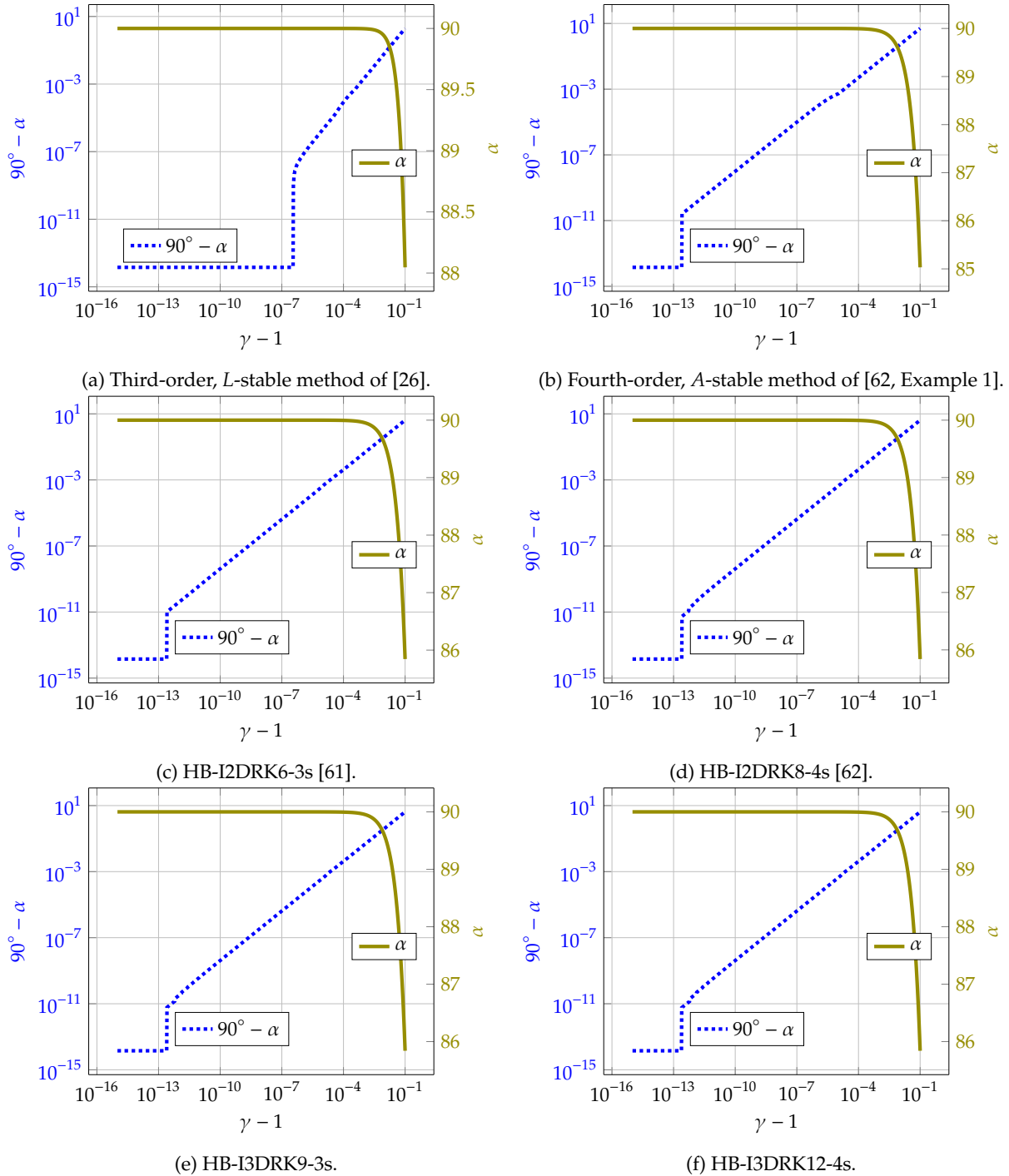


Figure 1: Angles of $A(\alpha)$ -stability for the relaxed update with fixed relaxation parameter $\gamma > 1$ for some implicit multiderivative methods.

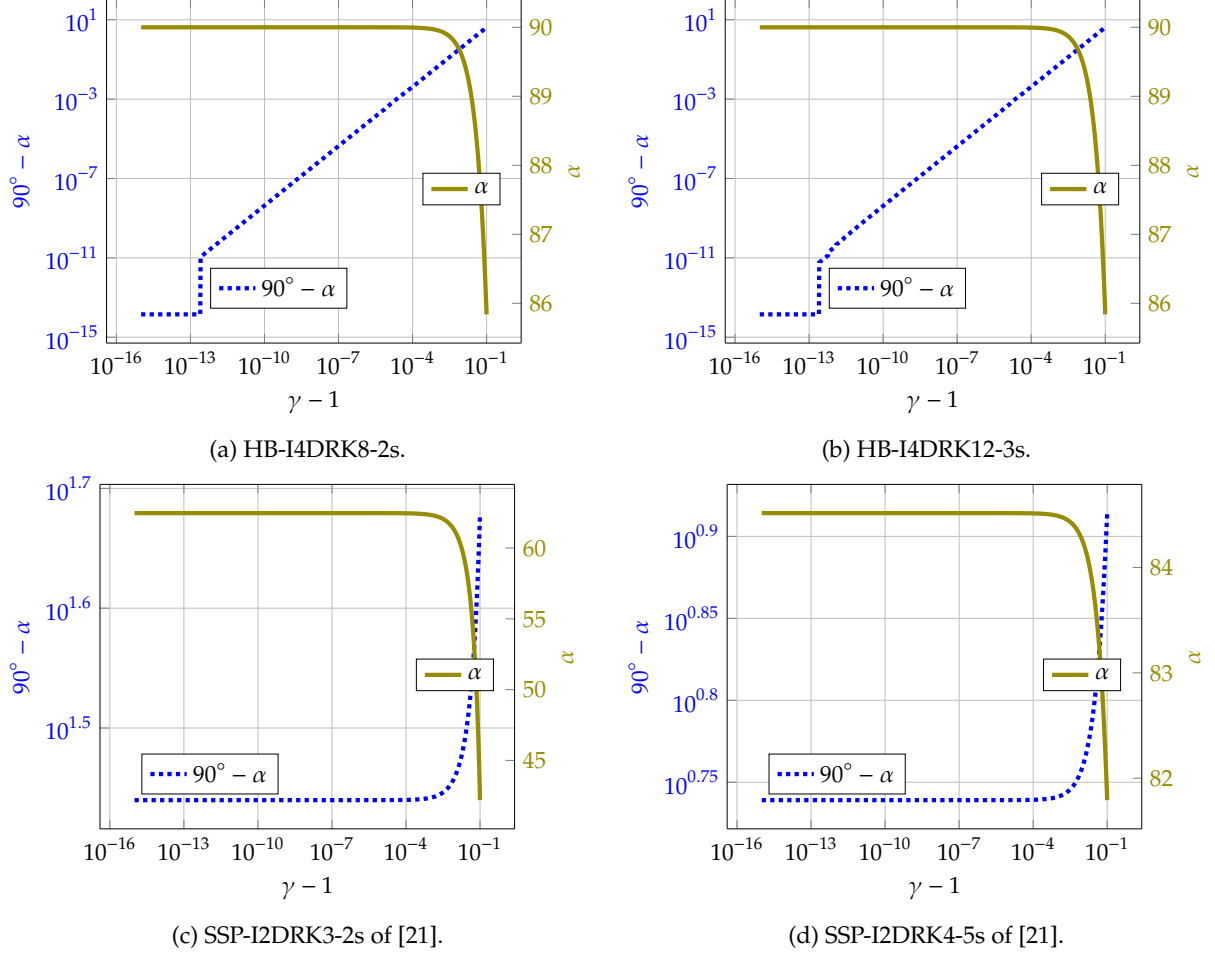


Figure 2: Angles of $A(\alpha)$ -stability for the relaxed update with fixed relaxation parameter $\gamma > 1$ for some implicit multiderivative methods.

the 3D compressible Euler equations of fluid dynamics to demonstrate the robustness of our approach as well as two nonlinear dispersive wave equations where the conservation of functionals is crucial to obtain better qualitative and quantitative results.

5.1. Convergence experiment I: a nonlinear oscillator

First, we demonstrate the convergence properties of the multiderivative methods with and without relaxation. We choose the entropy-conservative nonlinear oscillator

$$u'(t) = \frac{1}{\|u(t)\|^2} \begin{pmatrix} -u_2(t) \\ u_1(t) \end{pmatrix}, \quad \text{for } t \in (0, T), \quad u(0) = \begin{pmatrix} 1 \\ 0 \end{pmatrix}, \quad (5.1)$$

of [30, 42, 47] and its dissipative counterpart

$$u'(t) = \frac{1}{\|u(t)\|^2} \begin{pmatrix} -u_2(t) \\ u_1(t) \end{pmatrix} - \varepsilon \begin{pmatrix} u_1(t) \\ u_2(t) \end{pmatrix}, \quad \text{for } t \in (0, T), \quad u(0) = \begin{pmatrix} 1 \\ 0 \end{pmatrix}, \quad (5.2)$$

with analytical solution

$$u(t) = r(t) \begin{pmatrix} \cos \varphi(t) \\ \sin \varphi(t) \end{pmatrix}, \quad r(t) = \exp(-\varepsilon t), \quad \varphi(t) = \begin{cases} t, & \varepsilon = 0, \\ \frac{\exp(2\varepsilon t) - 1}{2\varepsilon}, & \varepsilon \neq 0. \end{cases} \quad (5.3)$$

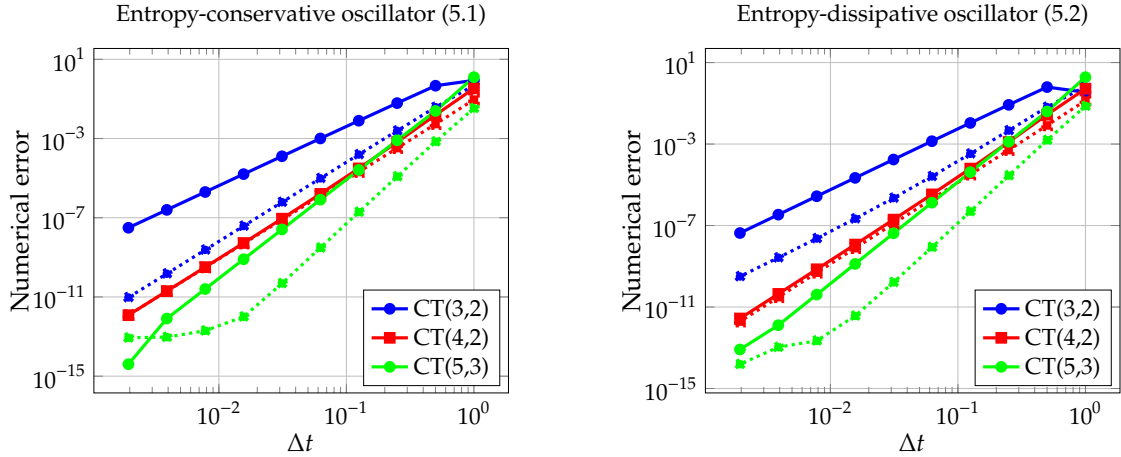


Figure 3: Convergence results for the nonlinear oscillators using the explicit third, fourth and fifth order methods of [13], see also Sec. A.1. Dotted lines correspond to the relaxed schemes, straight lines to the baseline schemes.

For the entropy-dissipative nonlinear oscillator, we choose the damping coefficient $\varepsilon = 10^{-2}$. In both cases, we choose the entropy $\eta(u) = \|u\|^2$ with the standard Euclidean inner product norm $\|\cdot\|$.

The errors at the final time $T = 10$ of the three explicit two-derivative methods CT(3,2), CT(4,2) and CT(5,3) from [13], see also Sec. A.1, are shown in Figure 3. The entropy estimation η^{new} has been computed using the four-point Gauss-Lobatto rule combined with the quintic polynomial outlined in (3.6). Note that the CT-methods are not collocation-based, so it is not obvious how to choose a continuous output.

We can clearly observe the expected orders of convergence of 3, 4, and 5 for the baseline schemes (straight lines). For the entropy-conservative case, the odd order methods show an increase in order. This phenomenon is well-known, and has been analyzed in [48]. In any case, also for the entropy-dissipative one, the relaxed methods of odd order behave significantly better than the baseline methods in that the error coefficients seem to be significantly smaller. For the fourth-order scheme, this difference is less pronounced; it is only visible for large timesteps.

Having considered explicit schemes, we now turn our attention to the class of implicit schemes. In particular, we consider some collocation-based schemes, see Sec. A.4, and a third-order SSP scheme (SSP-I2DRK3-2s) recently introduced in [21], see also Eq. (A.6). Numerical results have been reported in Fig. 4. Again, design orders of accuracy are visible for the baseline schemes in all cases. The third-order SSP scheme profits a lot from relaxation, which was to be expected, as the order is increased by one. For the other two methods, the difference between relaxed and baseline scheme is less pronounced.

For the entropy-dissipative case and the collocation-based schemes, we have computed η^{new} in two different fashions as explained in Sec. 3.1. An estimate is obtained through an appropriate Gauss-Lobatto quadrature combined with a *polynomial interpolation* (dotted) or a *continuous output* (dashed). For the sixth-order scheme, a Gauss-Lobatto quadrature with five points is used to obtain the appropriate order. As the SSP scheme does not come with a continuous output, there, only an estimate via interpolation was possible to obtain. It is very difficult to distinguish the dotted and the dashed lines in Fig. 4 (right). While they are not the same, they lie practically on top of each other, from which one can conclude that the results are not very sensitive to the choice of entropy estimator.

Error growth in time for nonlinear oscillators Here, we take a closer look at the behavior of the error of the three selected multiderivative Runge-Kutta methods by Chan and Tsai [13] for the nonlinear oscillators described in the previous subsection. The final time is set to $T = 125$

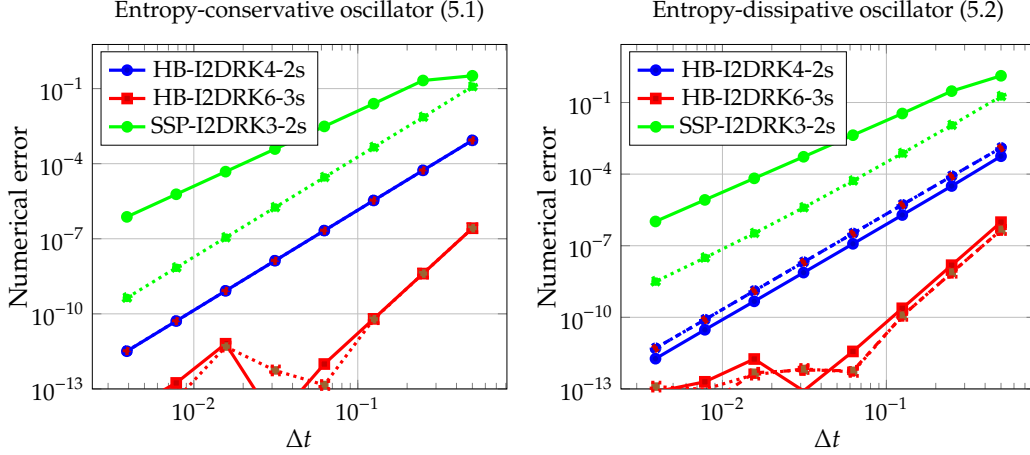


Figure 4: Convergence results for the nonlinear oscillators using several implicit schemes, see also Sec. A.3 and Sec. A.4. Straight lines correspond to the baseline schemes, while dotted and dashed lines use relaxation. For the entropy-conservative case, only dotted lines are plotted, as $\eta^{\text{new}} \equiv \eta(u^n)$ is trivial to obtain. For the entropy-dissipative case, estimating η^{new} is an important part of the algorithm, see Sec. 3.1. Dotted means that the estimate of η^{new} has been obtained using a Hermite-Birkhoff interpolation of u , while dashed means that the estimate has been obtained using the continuous Runge-Kutta output. Please note that the latter is not possible for the SSP scheme.

(entropy-conservative) and $T = 30$ (entropy-dissipative), and the rather large timestep of $\Delta t = 0.5$ is chosen. The results for the entropy-conservative nonlinear oscillator (5.1) are shown in Figure 5 on the top. Clearly, the relaxation approach conserves the entropy (up to machine accuracy) while the baseline scheme results in an either monotonically increasing or monotonically decreasing entropy. The error of the relaxation method grows linearly in time while the baseline scheme results in a quadratic asymptotic error growth in time, at least until the errors are so large that the numerical solution turns out to be useless. This is something that we can only see for the baseline scheme, relaxation clearly improves the long-time behaviour of the error.

The different behavior of the error growth in time can be understood, e.g., using the theory of [10, 12, 15]. Indeed, we are looking for a periodic orbit, which is a relative equilibrium solution of the Hamiltonian system (5.1). Thus, structure-preserving numerical methods are expected to result not only in improved qualitative behavior but also yield quantitatively better results due to a reduced error growth rate in time.

The corresponding results for the entropy-dissipative nonlinear oscillator (5.2) are shown in Figure 5 in the lower part. As expected for an accurate method and a strictly dissipative problem, the entropy decays over time. It is interesting to see that the relaxed method results in an entropy that is visually indistinguishable from the entropy of the analytical solution while the baseline methods clearly deviate. In addition, the error of the relaxed solution is smaller and grows slightly slower in time than the error of the baseline method. Since this problem is entropy-dissipative, it does not fit into the framework of [10, 12, 15] mentioned earlier. Nevertheless, applying relaxation still improves both the qualitative and quantitative behavior of the numerical solution.

The same investigation has been done for the implicit schemes mentioned in the previous convergence studies, see Fig. 6. Similar observations can be made. It has to be noted that, again, the third-order SSP scheme profits a lot from relaxation, which is visible both from the error growth and the evolution of η . For the even-order collocation schemes, this phenomenon is less pronounced. In particular, for these schemes, the quadratic functional η , in the entropy-conservative case, is conserved already for the baseline scheme. Obviously, this is also backed up by the findings from the convergence study in Fig. 4. A (small) advantage can be seen for the collocation schemes in the entropy-dissipative case.

For the entropy-dissipative case, we estimated η^{new} only through a Hermite-Birkhoff interpolation, as previous investigation has shown that the effect is negligible.

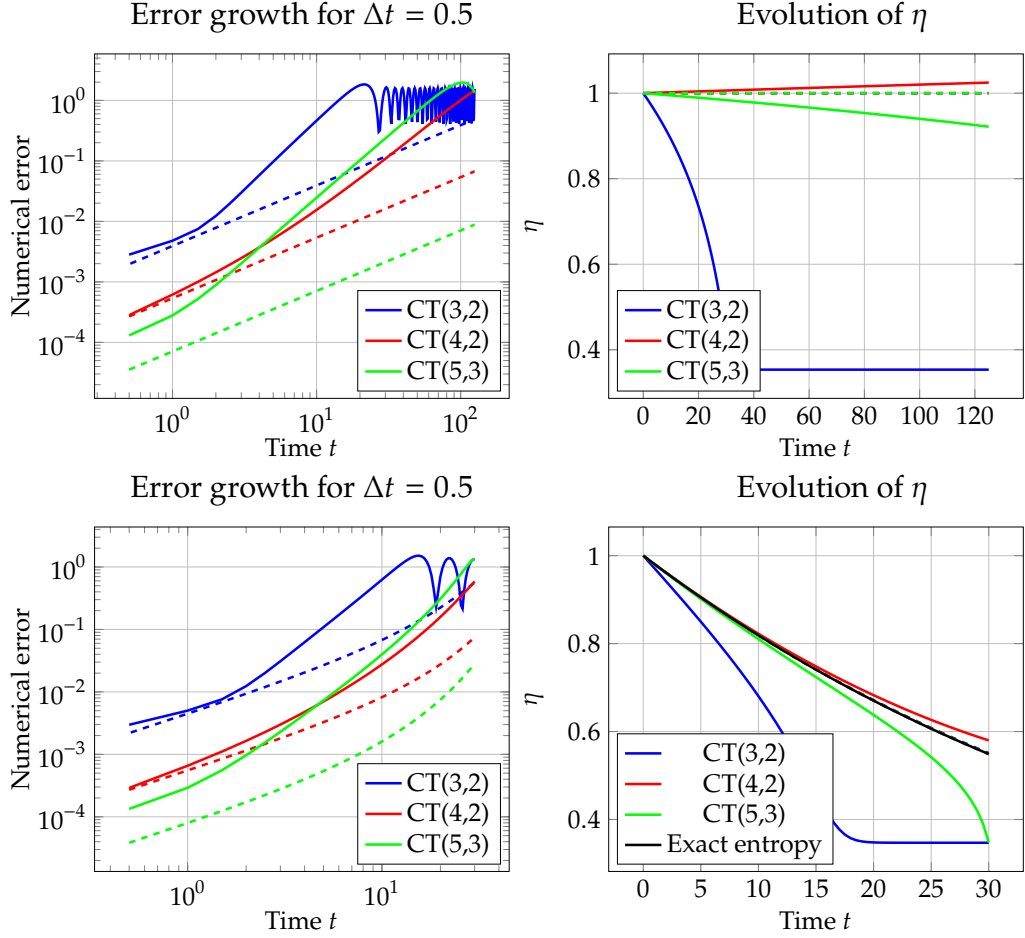


Figure 5: Temporal evolution of the numerical error and the functional η for the nonlinear oscillators using the explicit third, fourth and fifth order methods of [13], see also Sec. A.1. Top: conservative case (5.1), bottom: dissipative case (5.2). Dashed lines denote schemes that use relaxation.

5.2. Convergence experiment II: Kepler's problem

As a second test problem with a non-quadratic entropy, we discuss Kepler's problem following [49], which is given by

$$q'_i(t) = p_i(t), \quad p'_i(t) = -\frac{q_i(t)}{\|q(t)\|^3}, \quad i \in \{1, 2\}. \quad (5.4)$$

Here, $q: \mathbb{R}^+ \rightarrow \mathbb{R}^2$ and $p: \mathbb{R}^+ \rightarrow \mathbb{R}^2$ are the unknown functions. We choose the same initial conditions as in [49], i.e.,

$$q(0) = (1 - e, 0)^T, \quad p(0) = \left(0, \sqrt{\frac{1 - e}{1 + e}}\right)^T,$$

with eccentricity $e = \frac{1}{2}$. As "entropy" functional η , we choose the angular momentum

$$\eta(q, p) := q_1 p_2 - q_2 p_1,$$

which, for the exact solution, is a conserved quantity.

As in the previous section, we start with the class of explicit schemes from [13]; and we add two third-derivative schemes from [65] to demonstrate that our approach is independent of the number of derivatives. Numerical results have been plotted in Fig. 7 for a final time of $T = 5$. As η is not a

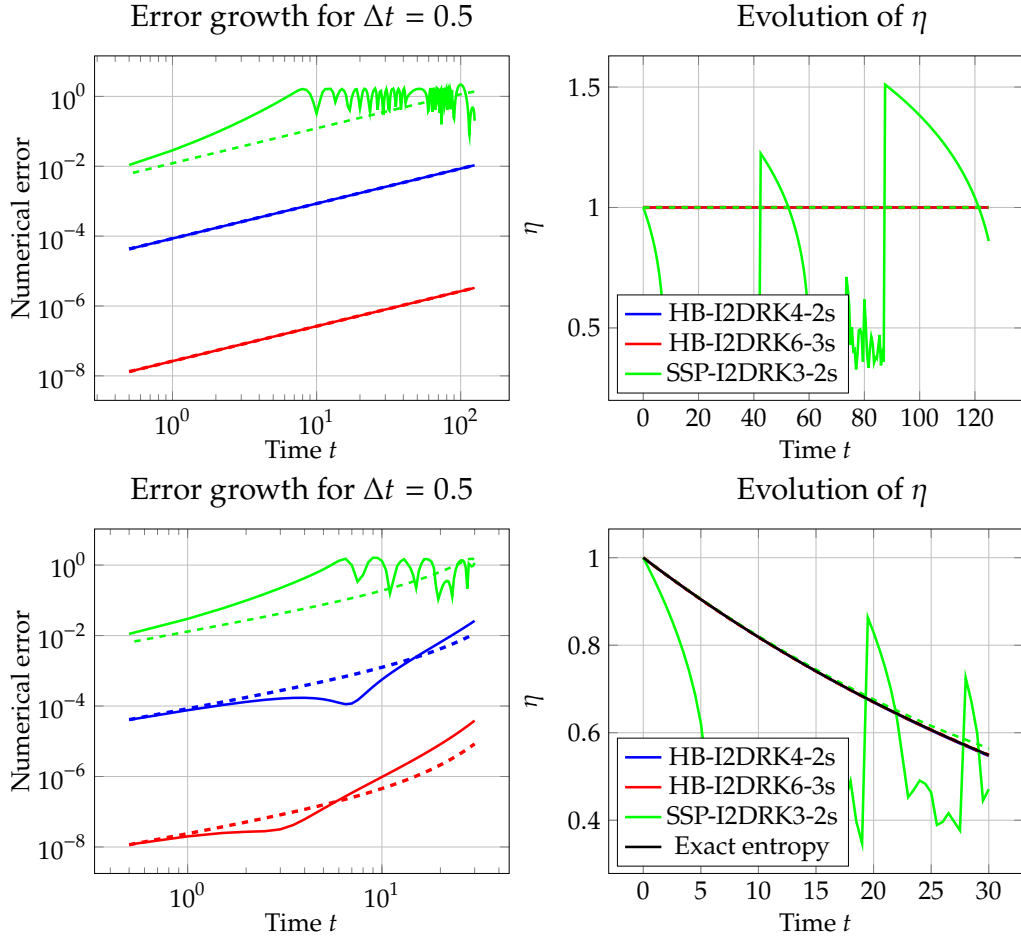


Figure 6: Temporal evolution of the numerical error and the functional η for the nonlinear oscillators using several implicit schemes, see also Sec. A.3 and Sec. A.4. Straight lines correspond to the baseline schemes, while dashed lines use relaxation. Top: conservative case (5.1), bottom: dissipative case (5.2). As the actual way how η^{new} is computed for the entropy-dissipative case turned out to have a negligible effect, only the Hermite-Birkhoff interpolation of u is used. Note that the baseline schemes for HB-I2DRK4-2s and HB-I2DRK6-3s are already excellent at preserving the functional for the entropy-conservative case, which is why it seems like there is only one plotted line. This is also very much in line with the convergence results from Fig. 4. The legend on the right is also valid for the figure on the left.

quadratic functional, we do not expect superconvergence and, indeed, both baseline and relaxed methods come with their design order of accuracy. However, we can repeat our observation for the odd-order schemes from the previous section, which is that the errors are typically lower, sometimes even significantly lower, and that the asymptotic regime is reached faster.

Fig. 8 shows convergence results for a couple of implicit collocation-based schemes of orders three, eight, and twelve, with up to four derivatives. Due to the relatively high order of the schemes involved, the final time has been increased to $T = 50$. On the left, baseline schemes are plotted, while on the right, the relaxed versions are displayed. Design accuracies are met, with the exception of the baseline scheme of order three that has not reached the asymptotic regime yet. (It has been checked that it converges, though.) Again, the relaxed version seems to reach the asymptotic regime way faster. Please note that as η is not quadratic any more, the functional is not preserved exactly by the baseline schemes, but it is by the relaxed schemes.

Error growth in time for Kepler's problem Similar as before, we show the behaviour of the error and the functional η as a function of time, exemplarily for the explicit schemes of Chan and Tsai [13], see also Sec. A.1, and Turaci and Öziş [65], see also Sec. A.2. Findings have been plotted in

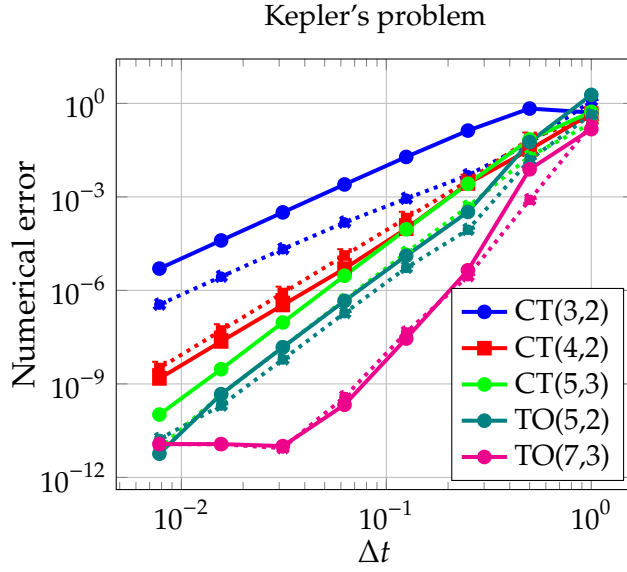


Figure 7: Convergence results for Kepler's problem (5.4) using the explicit third, fourth and fifth order methods of [13], see also Sec. A.1; and the three-derivative schemes of order 5 and 7 of Turaci and Öziş [65], see also Sec. A.2. Dotted lines correspond to the relaxed schemes, straight lines to the baseline schemes.

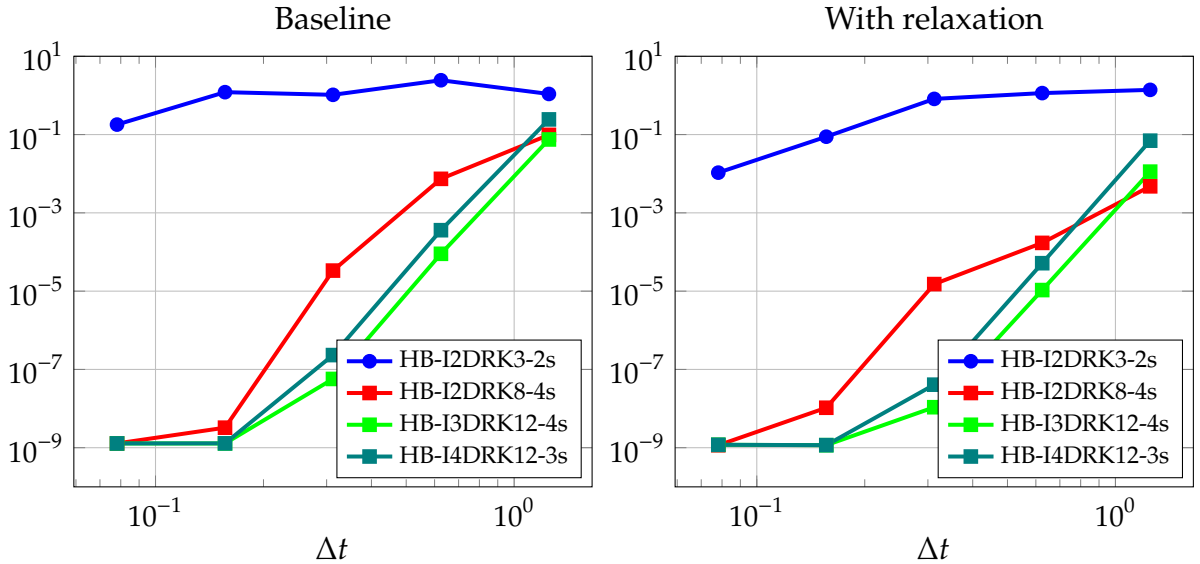


Figure 8: Several multiderivative timesteppers applied to the entropy conserving Kepler problem for various values of k_{\max} . The final end time has been set to $T = 50$ to account for the rather high order of the schemes involved (three, eight, twelve and twelve, respectively). The left figure displays the baseline schemes, while the right figure displays the schemes with a relaxation. Convergence stalls relatively early due to the used, numerically computed, reference solution, which obviously tends to become less accurate with larger final time T .

Fig. 9. On the left, error evolution over time and on the right, functional evolution over time have been plotted. In all the cases, the baseline scheme behaves worse than its relaxed counterpart.

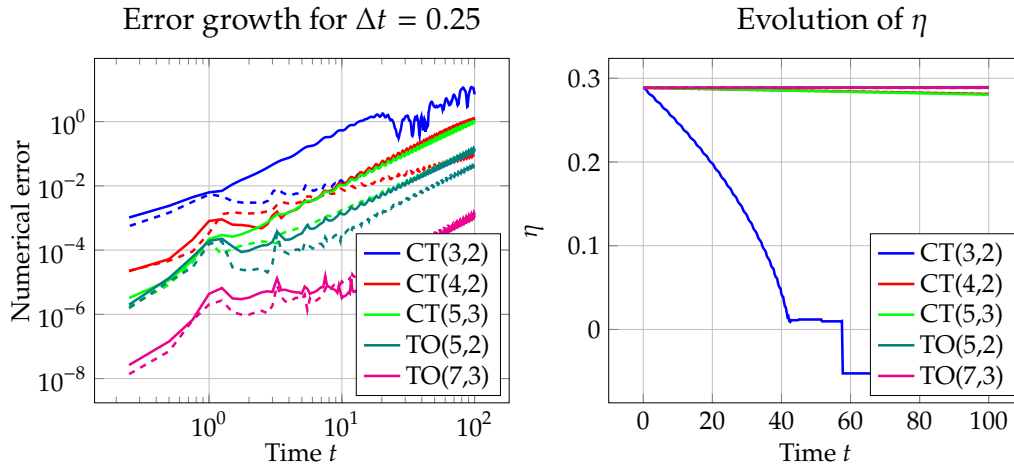


Figure 9: Temporal evolution of the numerical error and the functional η for Kepler's problem (5.4) using the explicit third, fourth and fifth order methods of [13], see also Sec. A.1; and the three-derivative schemes of order 5 and 7 of Turaci and Öziş [65], see also Sec. A.2. Dotted lines correspond to the relaxed schemes, straight lines to the baseline schemes.

5.3. Convergence experiment III: dissipated exponential entropy

As a final ODE problem, we consider an admittedly rather artificial equation with a non-quadratic dissipative entropy. The problem is taken from [49], it is given by the equation

$$u'(t) = -e^{u(t)}, \quad u(0) = 0.5. \quad (5.5)$$

For all results, final time has been set to $T = 2.5$.

For the nonlinear functional $\eta(u) = e^u$, it is straightforward to check that solutions to (5.5) fulfill $\frac{d}{dt}\eta(u) \leq 0$.

In Fig. 10, convergence results for a variety of methods have been plotted. First of all, the findings from the previous sections are valid for this testcase as well. As we are dealing with a dissipative rather than a conservative case, it is to be expected that the quality of the solution does not improve dramatically by introducing relaxation, which is also visible from Fig. 10. In fact (not plotted here), already the baseline schemes produce, in the range of Δt considered here, solutions with a decaying entropy η . The advantage of using a relaxed scheme is that one can be absolutely certain, in a mathematically rigorous way, that the functional decays. Please note that, in contrast to previous findings, the relaxed schemes have a slightly higher error constant here. Also for this case, continuous output versus Hermite-Birkhoff interpolation in estimating η^{new} has been tested; the differences are not significant and hence not shown here.

5.4. 3D inviscid Taylor-Green vortex

Next, we demonstrate the robustness of the methods for a 3D simulation of compressible turbulence. For this, we consider the 3D compressible Euler equations of an ideal gas with ratio of specific heats $\gamma = 1.4$ and choose the classical inviscid Taylor-Green vortex initial data [20]

$$\begin{aligned} \varrho &= 1, \quad v_1 = \sin(x_1) \cos(x_2) \cos(x_3), \quad v_2 = -\cos(x_1) \sin(x_2) \cos(x_3), \quad v_3 = 0, \\ p &= \frac{\varrho^0}{\text{Ma}^2 \gamma} + \varrho^0 \frac{\cos(2x_1) \cos(2x_3) + 2 \cos(2x_2) + 2 \cos(2x_1) + \cos(2x_2) \cos(2x_3)}{16}, \end{aligned} \quad (5.6)$$

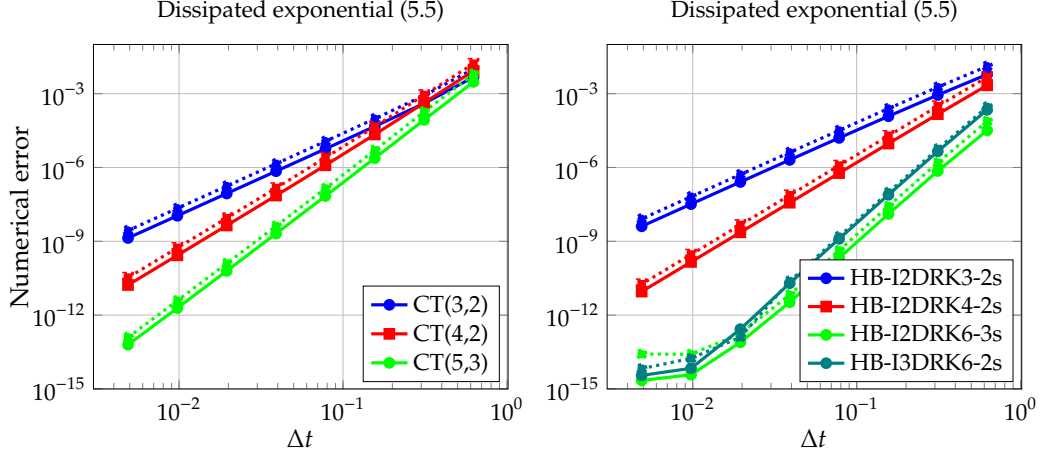


Figure 10: Convergence results for the dissipated exponential problem (5.5). Left: explicit third, fourth and fifth order methods of [13], see also Sec. A.1; and the three-derivative schemes of order 5 and 7 of Turaci and Öziş [65], see also Sec. A.2, are used. Right: some implicit collocation-based schemes. Dotted lines correspond to the relaxed schemes, straight lines to the baseline schemes.

with Mach number $Ma = 0.1$, density ρ , velocity v , and pressure p . The domain $[-\pi, \pi]^3$ is equipped with periodic boundary conditions. The spatial semidiscretization is performed using flux differencing DG methods, specifically the discontinuous Galerkin spectral element method (DGSEM) on tensor product elements using the Gauss-Lobatto-Legendre nodes with 8^3 uniform elements and polynomials of degree $p = 3$, resulting in 32768 degrees of freedom (DOFs). We use the entropy-conservative flux of [40, 41, 45] in the volume; the surface flux is either the same entropy-conservative flux or a dissipative local Lax-Friedrichs/Rusanov numerical flux. See [17, 20, 53] for a description of these methods.

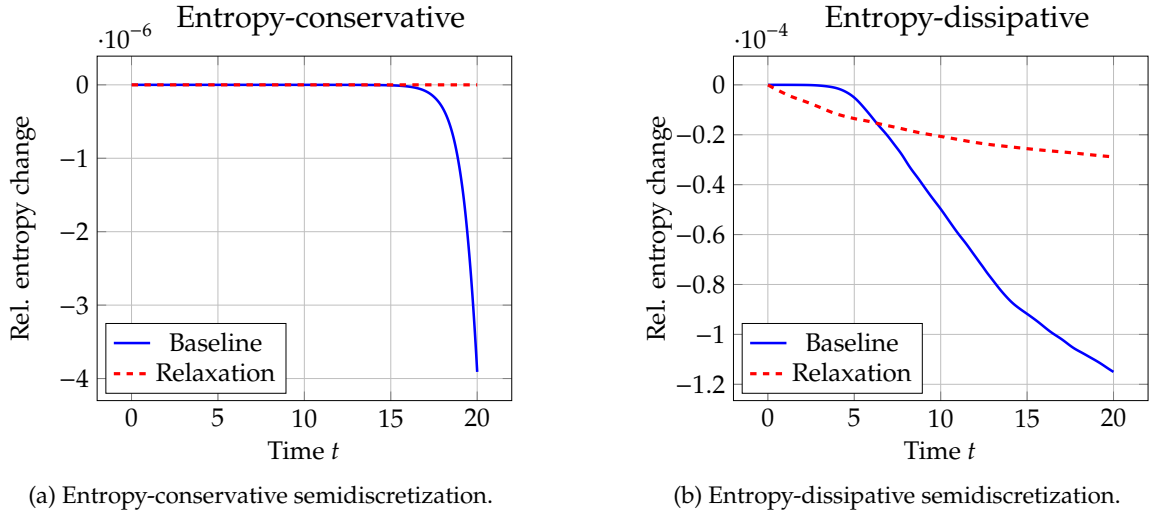


Figure 11: Numerical results for the 3D inviscid Taylor-Green vortex using discontinuous Galerkin methods in space and the explicit fourth-order, two-derivative method of [13] in time. Shown is the relative change of the entropy $(\eta(u) - \eta(u^0))/|\eta(u^0)|$.

We choose the classical physical entropy of the compressible Euler equations given by

$$\int -\frac{\rho s}{\gamma - 1}, \quad s = \log \frac{p}{\rho^\gamma}, \quad (5.7)$$

and its numerical realization via the collocation quadrature rule associated with the DGSEM. The entropy of numerical solutions obtained by the fourth-order, two-derivative method of [13]

with time step size $\Delta t = 0.005$ is shown in Figure 11². Clearly, the baseline method yields a visible change of the entropy over time in the entropy-conservative case while relaxation is able to conserve the entropy as expected. In the entropy-dissipative case, the baseline time integration method yields less dissipation initially but more dissipation for larger times. This numerical experiment demonstrates the robustness of the method even when combined with highly-nonlinear discretizations of PDEs and complicated entropy functionals.

5.5. Benjamin-Bona-Mahony equation

Next, we consider solitary wave solutions of the Benjamin-Bona-Mahony (BBM) equation [5]

$$\partial_t u + \partial_x u + \partial_x \frac{u^2}{2} - \partial_x^2 \partial_t u = 0. \quad (5.8)$$

We choose the spatial domain $[-90, 90]$ equipped with periodic boundary conditions and an initial condition corresponding to the solitary wave solution

$$u(t, x) = \frac{A}{\cosh(K(x - ct))^2}, \quad \text{with } A = 3(c - 1), \quad K = \frac{1}{2}\sqrt{1 - 1/c}, \quad c = 1.2. \quad (5.9)$$

We use the method-of-lines approach and combine an entropy-conservative semidiscretization of [51] with the two-derivative Runge-Kutta method (A.2) of [13]. The schemes conserve a discrete equivalent of the invariant

$$\int \left(u(t, x)^2 + (\partial_x u(t, x))^2 \right) dx. \quad (5.10)$$

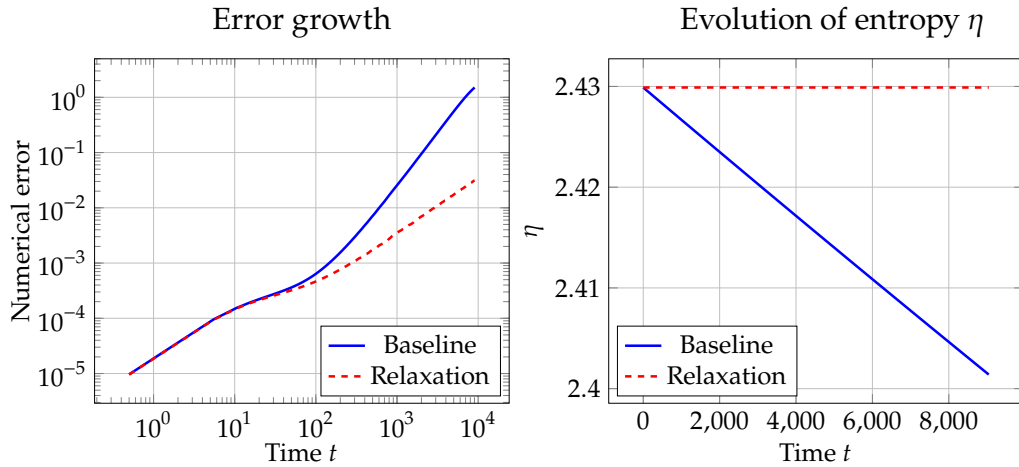


Figure 12: Numerical results for the BBM equation (5.8) discretized in space using an entropy-conservative Fourier collocation method with 2^8 nodes [51] and using the fourth-order method CT(4,2) of [13] with $\Delta t = 0.5$ in time.

The numerical results are shown in Figure 12. Clearly, the relaxation method conserves the entropy while the baseline scheme is entropy-dissipative in this case. The asymptotic error growth is linear for the relaxed method and quadratic for the baseline scheme. This behavior is expected based on the theory of [3], which is an extension of the relative equilibrium theory of [15] to Hamiltonian PDEs. Such a property has first been proved rigorously for the Korteweg-de Vries equation in [14] and later been extended to other equations such as the nonlinear Schrödinger equation [16]. The general framework also covers many other nonlinear dispersive wave equations [50].

²Since the time step size of explicit methods is limited by stability for this problem, an adaptive choice of the step sizes typically leads to an asymptotically constant Δt [46].

5.6. Korteweg-de Vries equation

Here, we consider the Korteweg-de Vries-equation, which is a third-order nonlinear partial differential equation, given by

$$u_t + \left(\frac{u^2}{2}\right)_x + u_{xxx} = 0, \quad (x, t) \in \mathbb{R} \times \mathbb{R}^+, \quad (5.11)$$

$$u(0, x) = u_0(x), \quad x \in \mathbb{R}. \quad (5.12)$$

Please note that this is, due to the occurrence of both nonlinear and third-order terms, a rather complex testcase. In particular, the term u_{xxx} has eigenvalues on the imaginary axis. There exists an exact soliton solution to this equation [14], given by

$$u(t, x) = 2 \cosh\left(\frac{\tilde{x}}{\sqrt{6}}\right)^{-2},$$

where we have defined \tilde{x} to be

$$\tilde{x} = \text{mod}\left(x - \frac{2t}{3}, 80\right) - 40.$$

The solution u on \mathbb{R} is hence a periodic repetition of the solution at, e.g., $x \in [0, 80]$, which is the domain that we actually discretize, with periodic boundary conditions, in our work. The time period is given by $T_{\text{per}} = \frac{3 \cdot 80}{2} = 120$. The discretization is done through a 17-point stencil Lagrangian finite difference scheme on a grid with 1000 elements, rendering the spatial resolution relatively high. It is evident both from the character of the Korteweg-de Vries equation and the high-order discretization that implicit schemes are an absolute necessity here. For the spatial discretization, the Burgers-term $(u^2/2)_x$ in (5.11) has been rewritten in the equivalent (at least for smooth solutions) split-form

$$\frac{1}{2}(u^2)_x \equiv \frac{1}{3}(u^2)_x + \frac{1}{3}uu_x.$$

This form has been used as with this form, it is straightforward to show that the functional

$$\eta(u) = \int_{\mathbb{R}} u^2 dx \quad (5.13)$$

is preserved.

Fig. 13 shows convergence results for three implicit schemes, always as baseline and relaxation scheme. The final time has been set as a rather short $T = 10$ on the left, and $T = 360$ on the right. $T = 360$ corresponds to three temporal periods of the solution. As before, only little difference can be seen for the HB-I2DRK4-2s and the HB-I2DRK6-3s scheme in their baseline and relaxed version. However, the behavior of the HB-I2DRK3-2s scheme is very interesting. For the smaller time $T = 10$, the relaxed version converges with third order, while for the larger time $T = 360$, it converges with fourth order rather than three, which is the baseline scheme's order. Obviously, this is a very odd behavior that one would not have anticipated. Hence, in Fig. 14, we have plotted for this particular scheme the error as a function of time for the baseline scheme (left) and the relaxed scheme (right) for various values of Δt . The error distribution for the baseline scheme is relatively smooth, and from about $t = 10$ on, it behaves quadratically in time. This is not true for the relaxed scheme, where there is a relatively long 'plateau' phase, after which the error grows linearly in time, in accordance with the analysis of [14]. This plateau phase seems to last longer, the smaller the timestep Δt is. This behavior, in our opinion, explains the different orders that we see here. In any case, it can be said that for HB-I2DRK3-2s, the relaxed scheme behaves significantly better than the unrelaxed one.

There are no SSP results, as we observed severe stability issues in this case. This can of course be explained from the relatively low stability angles as observed in Fig. 2.

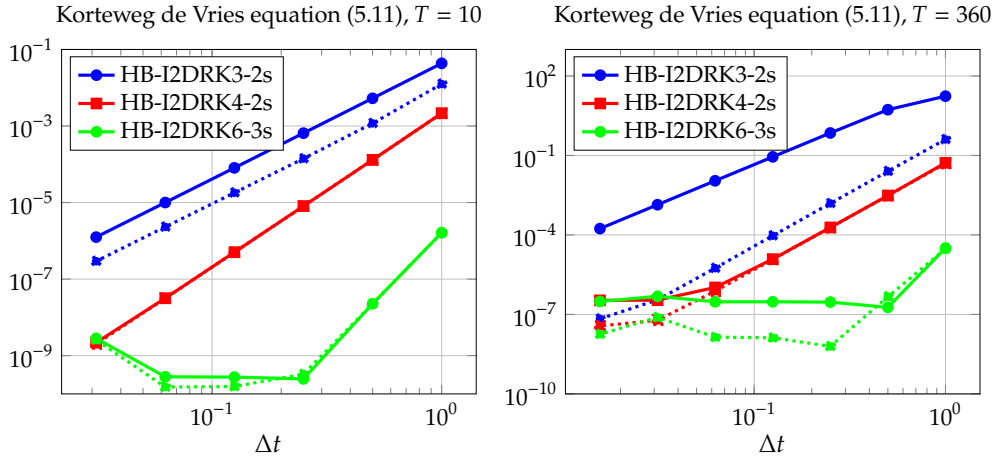


Figure 13: Convergence results for the Korteweg de Vries equation (5.11). Shown are the outputs of some implicit collocation-based schemes. Left: Final time $T = 10$, right: final time $T = 360$. Dotted lines correspond to the relaxed schemes, straight lines to the baseline schemes. For the HB-I2DRK4-2s scheme, baseline and relaxation scheme lie on top of each other; for the HB-I2DRK6-3s scheme, they are fairly close to each other.

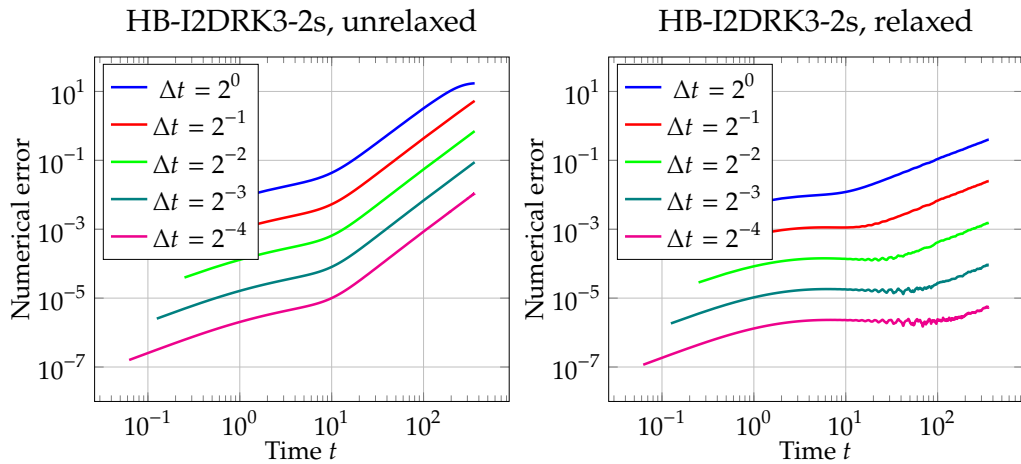


Figure 14: Temporal evolution of the numerical error for the Korteweg de Vries equation (5.11) discretized using the HB-I2DRK3-2s scheme for various timesteps Δt . Final time is $T = 360$, which corresponds to three temporal periods of the solution. Left: Baseline scheme, right: relaxed scheme. The fact that the curves start at different positions on the t -axis is due to the fact that $t = 0$ cannot be represented on this log-log-plot; the first data point is then at Δt .

6. Summary and conclusions

We have combined the recently developed relaxation approach to preserve important functionals (“entropies”) of numerical solutions of ODEs obtained by high-order multiderivative time integration methods with up to four temporal derivatives. Extending our previous work [56], we have considered not only invariants but also dissipated functionals. The latter required the development of appropriate entropy estimates in Section 3.1. In addition, we have analyzed stability properties of multiderivative relaxation methods in Section 4. The numerical results of Section 5 have demonstrated the robustness of the approach as well as qualitative and quantitative improvements of numerical solutions.

Future work in this direction will concentrate on energy-stable DG discretizations of the Cahn-Hilliard equation using a relaxation approach. Furthermore, numerical results have shown that some even-order collocation-based multiderivative schemes seem to handle quadratic entropies very well. A theoretical and practical study of the implications here will be performed.

Acknowledgments

HR was supported by the Deutsche Forschungsgemeinschaft (DFG, German Research Foundation, project number 513301895) and the Daimler und Benz Stiftung (Daimler and Benz foundation, project number 32-10/22).

References

- [1] A. Abdi and D. Conte. “Implementation of second derivative general linear methods.” In: *Calcolo* 57.20 (2020). DOI: 10.1007/s10092-020-00370-w.
- [2] R. Abgrall, E. L. Méledo, P. Öffner, and D. Torlo. “Relaxation Deferred Correction Methods and their Applications to Residual Distribution Schemes.” In: *The SMAI Journal of Computational Mathematics* 8 (2022), pp. 125–160. DOI: 10.5802/smai-jcm.82. arXiv: 2106.05005 [math.NA].
- [3] A Araújo and A. Durán. “Error propagation in the numerical integration of solitary waves. The regularized long wave equation.” In: *Applied Numerical Mathematics* 36.2-3 (2001), pp. 197–217. DOI: 10.1016/S0168-9274(99)00148-8.
- [4] A. Babbar, S. K. Kenettinkara, and P. Chandrashekar. “Lax-Wendroff flux reconstruction method for hyperbolic conservation laws.” In: *Journal of Computational Physics* 467.111423 (2022). DOI: 10.1016/j.jcp.2022.111423. arXiv: 2207.02954 [math.NA].
- [5] T. B. Benjamin, J. L. Bona, and J. J. Mahony. “Model equations for long waves in nonlinear dispersive systems.” In: *Philosophical Transactions of the Royal Society of London. Series A, Mathematical and Physical Sciences* 272.1220 (1972), pp. 47–78. DOI: 10.1098/rsta.1972.0032.
- [6] J. Bezanson, A. Edelman, S. Karpinski, and V. B. Shah. “Julia: A Fresh Approach to Numerical Computing.” In: *SIAM Review* 59.1 (2017), pp. 65–98. DOI: 10.1137/141000671. arXiv: 1411.1607 [cs.MS].
- [7] A. Biswas and D. I. Ketcheson. *Accurate Solution of the Nonlinear Schrödinger Equation via Conservative Multiple-Relaxation ImEx Methods*. 2023. arXiv: 2309.02324 [math.NA].
- [8] A. Biswas and D. I. Ketcheson. “Multiple relaxation Runge-Kutta methods for conservative dynamical systems.” In: *Journal of Scientific Computing* 97.4 (2023). DOI: 10.1007/s10915-023-02312-4.
- [9] M. Calvo, D. Hernández-Abreu, J. I. Montijano, and L. Rández. “On the Preservation of Invariants by Explicit Runge-Kutta Methods.” In: *SIAM Journal on Scientific Computing* 28.3 (2006), pp. 868–885. DOI: 10.1137/04061979X.

- [10] M. Calvo, M. Laburta, J. I. Montijano, and L. Rández. “Error growth in the numerical integration of periodic orbits.” In: *Mathematics and Computers in Simulation* 81.12 (2011), pp. 2646–2661. doi: 10.1016/j.matcom.2011.05.007.
- [11] M. Calvo, M. Laburta, J. I. Montijano, and L. Rández. “Projection methods preserving Lyapunov functions.” In: *BIT Numerical Mathematics* 50.2 (2010), pp. 223–241. doi: 10.1007/s10543-010-0259-3.
- [12] B Cano and J. M. Sanz-Serna. “Error growth in the numerical integration of periodic orbits, with application to Hamiltonian and reversible systems.” In: *SIAM Journal on Numerical Analysis* 34.4 (1997), pp. 1391–1417. doi: 10.1137/S0036142995281152.
- [13] R. P. Chan and A. Y. Tsai. “On explicit two-derivative Runge-Kutta methods.” In: *Numerical Algorithms* 53 (2010), pp. 171–194. doi: 10.1007/s11075-009-9349-1.
- [14] J De Frutos and J. M. Sanz-Serna. “Accuracy and conservation properties in numerical integration: the case of the Korteweg-de Vries equation.” In: *Numerische Mathematik* 75.4 (1997), pp. 421–445. doi: 10.1007/s002110050247.
- [15] A. Durán and J. M. Sanz-Serna. “The numerical integration of relative equilibrium solutions. Geometric theory.” In: *Nonlinearity* 11.6 (1998). doi: 10.1088/0951-7715/11/6/008.
- [16] A. Durán and J. M. Sanz-Serna. “The numerical integration of relative equilibrium solutions. The nonlinear Schrödinger equation.” In: *IMA Journal of Numerical Analysis* 20.2 (2000), pp. 235–261. doi: 10.1093/imanum/20.2.235.
- [17] T. C. Fisher and M. H. Carpenter. “High-order entropy stable finite difference schemes for nonlinear conservation laws: Finite domains.” In: *Journal of Computational Physics* 252 (2013), pp. 518–557. doi: 10.1016/j.jcp.2013.06.014.
- [18] M. Frigo and S. G. Johnson. “The design and implementation of FFTW3.” In: *Proceedings of the IEEE* 93.2 (2005), pp. 216–231. doi: 10.1109/JPROC.2004.840301.
- [19] E. Gaburro, P. Öffner, M. Ricchiuto, and D. Torlo. “High order entropy preserving ADER-DG scheme.” In: *Applied Mathematics and Computation* 440.127644 (2023). doi: 10.1016/j.amc.2022.127644. arXiv: 2206.03889 [math.NA].
- [20] G. J. Gassner, A. R. Winters, and D. A. Kopriva. “Split Form Nodal Discontinuous Galerkin Schemes with Summation-By-Parts Property for the Compressible Euler Equations.” In: *Journal of Computational Physics* 327 (2016), pp. 39–66. doi: 10.1016/j.jcp.2016.09.013.
- [21] S. Gottlieb, Z. J. Grant, J. Hu, and R. Shu. “High Order Strong Stability Preserving Multiderivative Implicit and IMEX Runge-Kutta Methods with Asymptotic Preserving Properties.” In: *SIAM Journal on Numerical Analysis* 60.1 (2022), pp. 423–449. doi: 10.1137/21M1403175.
- [22] S. Gottlieb, D. I. Ketcheson, and C.-W. Shu. *Strong stability preserving Runge-Kutta and multistep time discretizations*. Singapore: World Scientific, 2011.
- [23] E. Hairer and G. Wanner. “Multistep-multistage-multiderivative methods for ordinary differential equations.” In: *Computing (Arch. Elektron. Rechnen)* 11.3 (1973), pp. 287–303. doi: 10.1007/BF02252917.
- [24] E. Hairer, C. Lubich, and G. Wanner. *Geometric Numerical Integration: Structure-Preserving Algorithms for Ordinary Differential Equations*. Vol. 31. Springer Series in Computational Mathematics. Berlin Heidelberg: Springer-Verlag, 2006. doi: 10.1007/3-540-30666-8.
- [25] E. Hairer, S. P. Nørsett, and G. Wanner. *Solving Ordinary Differential Equations I: Nonstiff Problems*. Vol. 8. Springer Series in Computational Mathematics. Berlin Heidelberg: Springer-Verlag, 2008. doi: 10.1007/978-3-540-78862-1.
- [26] A. Jaust, J. Schütz, and D. C. Seal. “Implicit multistage two-derivative discontinuous Galerkin schemes for viscous conservation laws.” In: *Journal of Scientific Computing* 69 (2016), pp. 866–891. doi: 10.1007/s10915-016-0221-x.

- [27] S. Kang and E. M. Constantinescu. “Entropy-Preserving and Entropy-Stable Relaxation IMEX and Multirate Time-Stepping Methods.” In: *Journal of Scientific Computing* 93 (2022), p. 23. doi: 10.1007/s10915-022-01982-w. arXiv: 2108.08908 [math.NA].
- [28] K. Kastlunger and G. Wanner. “On Turan type implicit Runge-Kutta methods.” In: *Computing* 9 (1972), pp. 317–325. doi: 10.1007/BF02241605.
- [29] D. I. Ketcheson. “Relaxation Runge-Kutta Methods: Conservation and Stability for Inner-Product Norms.” In: *SIAM Journal on Numerical Analysis* 57.6 (2019), pp. 2850–2870. doi: 10.1137/19M1263662. arXiv: 1905.09847 [math.NA].
- [30] D. I. Ketcheson and H. Ranocha. “Computing with B-series.” In: *ACM Transactions on Mathematical Software* (Dec. 2022). doi: 10.1145/3573384. arXiv: 2111.11680 [math.NA].
- [31] P. Lax and B. Wendroff. “Systems of conservation laws.” In: *Communications on Pure and Applied Mathematics* 13.2 (1960), pp. 217–237. doi: 10.1002/cpa.3160130205.
- [32] T. Leibner and M. Ohlberger. “A new entropy-variable-based discretization method for minimum entropy moment approximations of linear kinetic equations.” In: *ESAIM: Mathematical Modelling and Numerical Analysis* 55.6 (2021), pp. 2567–2608. doi: 10.1051/m2an/2021065.
- [33] D. Li, X. Li, and Z. Zhang. “Implicit-explicit relaxation Runge-Kutta methods: construction, analysis and applications to PDEs.” In: *Mathematics of Computation* (2022). doi: 10.1090/mcom/3766.
- [34] D. Li, X. Li, and Z. Zhang. “Linearly implicit and high-order energy-preserving relaxation schemes for highly oscillatory Hamiltonian systems.” In: *Journal of Computational Physics* 111925 (2023). doi: 10.1016/j.jcp.2023.111925.
- [35] V. Linders, H. Ranocha, and P. Birken. “Resolving Entropy Growth from Iterative Methods.” In: *BIT Numerical Mathematics* (Sept. 2023). doi: 10.1007/s10543-023-00992-w. arXiv: 2302.13579 [math.NA].
- [36] MathWorks. *MATLAB*. Version R2022b. 2022. URL: <https://mathworks.com/products/matlab.html>.
- [37] D. Mitsotakis, H. Ranocha, D. I. Ketcheson, and E. Süli. “A conservative fully-discrete numerical method for the regularized shallow water wave equations.” In: *SIAM Journal on Scientific Computing* 42 (2 Apr. 2021). doi: 10.1137/20M1364606. arXiv: 2009.09641 [math.NA].
- [38] A. Moradi, A. Abdi, and J. Farzi. “Strong stability preserving second derivative general linear methods with Runge-Kutta stability.” In: *Journal of Scientific Computing* 85.1 (2020), Paper No. 1, 39. doi: 10.1007/s10915-020-01306-w. URL: <https://doi.org/10.1007/s10915-020-01306-w>.
- [39] A. Quarteroni, R. Sacco, and F. Saleri. *Numerical Mathematics*. Second Edition. Springer, 2007. doi: 10.1007/b98885.
- [40] H. Ranocha. “Comparison of Some Entropy Conservative Numerical Fluxes for the Euler Equations.” In: *Journal of Scientific Computing* 76.1 (July 2018), pp. 216–242. doi: 10.1007/s10915-017-0618-1. arXiv: 1701.02264 [math.NA].
- [41] H. Ranocha. “Entropy Conserving and Kinetic Energy Preserving Numerical Methods for the Euler Equations Using Summation-by-Parts Operators.” In: *Spectral and High Order Methods for Partial Differential Equations ICOSAHOM 2018*. Ed. by S. J. Sherwin, D. Moxey, J. Peiró, P. E. Vincent, and C. Schwab. Vol. 134. Lecture Notes in Computational Science and Engineering. Cham: Springer, Aug. 2020, pp. 525–535. doi: 10.1007/978-3-030-39647-3_42.
- [42] H. Ranocha. “On Strong Stability of Explicit Runge-Kutta Methods for Nonlinear Semi-bounded Operators.” In: *IMA Journal of Numerical Analysis* 41.1 (Jan. 2021), pp. 654–682. doi: 10.1093/imanum/drz070. arXiv: 1811.11601 [math.NA].

- [43] H. Ranocha. “SummationByPartsOperators.jl: A Julia library of provably stable semidiscretization techniques with mimetic properties.” In: *Journal of Open Source Software* 6.64 (Aug. 2021), p. 3454. doi: 10.21105/joss.03454. URL: <https://github.com/ranocha/SummationByPartsOperators.jl>.
- [44] H. Ranocha, L. Dalcin, and M. Parsani. “Fully-Discrete Explicit Locally Entropy-Stable Schemes for the Compressible Euler and Navier-Stokes Equations.” In: *Computers and Mathematics with Applications* 80.5 (July 2020), pp. 1343–1359. doi: 10.1016/j.camwa.2020.06.016. arXiv: 2003.08831 [math.NA].
- [45] H. Ranocha and G. J. Gassner. “Preventing pressure oscillations does not fix local linear stability issues of entropy-based split-form high-order schemes.” In: *Communications on Applied Mathematics and Computation* (Aug. 2021). doi: 10.1007/s42967-021-00148-z. arXiv: 2009.13139 [math.NA].
- [46] H. Ranocha and J. Giesselmann. *Stability of step size control based on a posteriori error estimates*. July 2023. doi: 10.48550/arXiv.2307.12677. arXiv: 2307.12677 [math.NA].
- [47] H. Ranocha and D. I. Ketcheson. “Energy Stability of Explicit Runge-Kutta Methods for Nonautonomous or Nonlinear Problems.” In: *SIAM Journal on Numerical Analysis* 58.6 (Nov. 2020), pp. 3382–3405. doi: 10.1137/19M1290346. arXiv: 1909.13215 [math.NA].
- [48] H. Ranocha and D. I. Ketcheson. “Relaxation Runge-Kutta Methods for Hamiltonian Problems.” In: *Journal of Scientific Computing* 84.1 (July 2020). doi: 10.1007/s10915-020-01277-y. arXiv: 2001.04826 [math.NA].
- [49] H. Ranocha, L. Lóczy, and D. I. Ketcheson. “General Relaxation Methods for Initial-Value Problems with Application to Multistep Schemes.” In: *Numerische Mathematik* 146 (Oct. 2020), pp. 875–906. doi: 10.1007/s00211-020-01158-4. arXiv: 2003.03012 [math.NA].
- [50] H. Ranocha, M. Quezada de Luna, and D. I. Ketcheson. “On the Rate of Error Growth in Time for Numerical Solutions of Nonlinear Dispersive Wave Equations.” In: *Partial Differential Equations and Applications* 2.6 (Oct. 2021), p. 76. doi: 10.1007/s42985-021-00126-3. arXiv: 2102.07376 [math.NA].
- [51] H. Ranocha, D. Mitsotakis, and D. I. Ketcheson. “A Broad Class of Conservative Numerical Methods for Dispersive Wave Equations.” In: *Communications in Computational Physics* 29.4 (Feb. 2021), pp. 979–1029. doi: 10.4208/cicp.0A-2020-0119. arXiv: 2006.14802 [math.NA].
- [52] H. Ranocha, M. Sayyari, L. Dalcin, M. Parsani, and D. I. Ketcheson. “Relaxation Runge-Kutta Methods: Fully-Discrete Explicit Entropy-Stable Schemes for the Compressible Euler and Navier-Stokes Equations.” In: *SIAM Journal on Scientific Computing* 42.2 (Mar. 2020), A612–A638. doi: 10.1137/19M1263480. arXiv: 1905.09129 [math.NA].
- [53] H. Ranocha, M. Schlottke-Lakemper, J. Chan, A. M. Rueda-Ramírez, A. R. Winters, F. Hindenlang, and G. J. Gassner. “Efficient implementation of modern entropy stable and kinetic energy preserving discontinuous Galerkin methods for conservation laws.” In: *ACM Transactions on Mathematical Software* (Sept. 2023). doi: 10.1145/3625559. arXiv: 2112.10517 [cs.MS].
- [54] H. Ranocha, M. Schlottke-Lakemper, A. R. Winters, E. Faulhaber, J. Chan, and G. J. Gassner. “Adaptive numerical simulations with Trixi.jl: A case study of Julia for scientific computing.” In: *Proceedings of the JuliaCon Conferences* 1.1 (Jan. 2022), p. 77. doi: 10.21105/jcon.00077. arXiv: 2108.06476 [cs.MS].
- [55] H. Ranocha and J. Schütz. *Reproducibility repository for “Multiderivative time integration methods preserving nonlinear functionals via relaxation”*. 2023_multiderivative_relaxation. 2023. doi: 10.5281/zenodo.10057727.
- [56] H. Ranocha, J. Schütz, and E. Theodosiou. “Functional-preserving predictor-corrector multiderivative schemes.” In: *Proceedings in Applied Mathematics and Mechanics* (Sept. 2023). doi: 10.1002/pamm.202300025. arXiv: 2308.04876 [math.NA].

- [57] J. Revels, M. Lubin, and T. Papamarkou. *Forward-Mode Automatic Differentiation in Julia*. July 2016. DOI: 10.48550/arXiv.1607.07892. arXiv: 1607.07892 [cs.MS].
- [58] J. M. Sanz-Serna. “An explicit finite-difference scheme with exact conservation properties.” In: *Journal of Computational Physics* 47.2 (1982), pp. 199–210. DOI: 10.1016/0021-9991(82)90074-2.
- [59] M. Schlottke-Lakemper, A. R. Winters, H. Ranocha, and G. J. Gassner. “A purely hyperbolic discontinuous Galerkin approach for self-gravitating gas dynamics.” In: *Journal of Computational Physics* 442 (June 2021), p. 110467. DOI: 10.1016/j.jcp.2021.110467. arXiv: 2008.10593 [math.NA].
- [60] J. Schütz and D. C. Seal. “An asymptotic preserving semi-implicit multiderivative solver.” In: *Applied Numerical Mathematics* 160 (2021), pp. 84–101. DOI: 10.1016/j.apnum.2020.09.004.
- [61] J. Schütz, D. C. Seal, and A. Jaust. “Implicit multiderivative collocation solvers for linear partial differential equations with discontinuous Galerkin spatial discretizations.” In: *Journal of Scientific Computing* 73 (2017), pp. 1145–1163. DOI: 10.1007/s10915-017-0485-9.
- [62] J. Schütz, D. C. Seal, and J. Zeifang. “Parallel-in-time high-order multiderivative IMEX solvers.” In: *Journal of Scientific Computing* 90.1 (2022), p. 54. DOI: 10.1007/s10915-021-01733-3.
- [63] D. C. Seal, Y. Güçlü, and A. J. Christlieb. “High-order multiderivative time integrators for hyperbolic conservation laws.” In: *Journal of Scientific Computing* 60 (2014), pp. 101–140. DOI: 10.1007/s10915-013-9787-8.
- [64] A. Y. Tsai, R. P. Chan, and S. Wang. “Two-derivative Runge-Kutta methods for PDEs using a novel discretization approach.” In: *Numerical Algorithms* 65 (2014), pp. 687–703. DOI: 10.1007/s11075-014-9823-2.
- [65] M. Ökten Turaci and T. Öziş. “Derivation of three-derivative Runge-Kutta methods.” In: *Numerical Algorithms* 74.1 (2017), pp. 247–265. DOI: 10.1007/s11075-016-0147-2.
- [66] P. Turán. “On the theory of the mechanical quadrature.” In: *Acta Universitatis Szegediensis Acta Scientiarum Mathematicarum* 12 (1950), pp. 30–37.
- [67] M. Waruszewski, J. E. Kozdon, L. C. Wilcox, T. H. Gibson, and F. X. Giraldo. “Entropy stable discontinuous Galerkin methods for balance laws in non-conservative form: Applications to the Euler equations with gravity.” In: *Journal of Computational Physics* 468 (2022), p. 111507. DOI: 10.1016/j.jcp.2022.111507. arXiv: 2110.15920 [math.NA].
- [68] J. Zeifang, J. Schütz, and D. C. Seal. “Stability of implicit multiderivative deferred correction methods.” In: *BIT Numerical Mathematics* (2022), pp. 1–17. DOI: 10.1007/s10543-022-00919-x.
- [69] J. Zeifang, A. Thenery Manikantan, and J. Schütz. “Time parallelism and Newton-adaptivity of the two-derivative deferred correction discontinuous Galerkin method.” In: *Applied Mathematics and Computation* 457.128198 (2023). DOI: 10.1016/j.amc.2023.128198.
- [70] H. Zhang, X. Qian, J. Yan, and S. Song. “Highly efficient invariant-conserving explicit Runge-Kutta schemes for nonlinear Hamiltonian differential equations.” In: *Journal of Computational Physics* (2020), p. 109598. DOI: 10.1016/j.jcp.2020.109598.

A. Butcher tableaux

Several multiderivative Runge-Kutta schemes have been used in this work. For convenience, we list them here in this appendix.

A.1. Third-, fourth-, and fifth-order schemes from Chan and Tsai [13]

$$\text{CT}(3,2): \begin{array}{c|cc|cc} 0 & & & & & \\ 1 & 1 & & & \frac{1}{2} & \\ \hline & \frac{2}{3} & \frac{1}{3} & & \frac{1}{6} & 0 \end{array} \quad (\text{A.1})$$

$$\text{CT}(4,2): \begin{array}{c|cc|cc} 0 & & & & & \\ \frac{1}{2} & \frac{1}{2} & & & \frac{1}{8} & \\ \hline & 1 & 0 & & \frac{1}{6} & \frac{1}{3} \end{array} \quad (\text{A.2})$$

$$\text{CT}(5,3): \begin{array}{c|ccc|ccc} 0 & & & & & & \\ \frac{2}{5} & \frac{2}{5} & & & \frac{2}{25} & & \\ 1 & 1 & & & \frac{-1}{4} & \frac{3}{4} & \\ \hline & 1 & 0 & 0 & \frac{1}{8} & \frac{25}{72} & \frac{1}{36} \end{array} \quad (\text{A.3})$$

A.2. Three-derivative schemes from Turaci and Öziş [65]

$$\text{TO}(5,2): \begin{array}{c|ccc|cc|cc} 0 & & & & & & & \\ \frac{2}{5} & \frac{2}{5} & 0 & & \frac{2}{25} & & \frac{4}{375} & \\ \hline & 1 & 0 & & \frac{1}{2} & 0 & \frac{1}{16} & \frac{5}{48} \end{array} \quad (\text{A.4})$$

$$\text{TO}(7,3): \begin{array}{c|ccc|ccc|ccc} 0 & & & & & & & & & \\ c_2 & c_2 & 0 & 0 & \frac{c_2^2}{2} & 0 & 0 & \frac{c_2^3}{6} & & \\ c_3 & c_3 & 0 & 0 & \frac{c_3^2}{2} & 0 & 0 & \frac{c_3^3}{6} - a_{32} & a_{32} & \\ \hline & 1 & 0 & 0 & \frac{1}{2} & 0 & 0 & \frac{1}{30} & \frac{1}{15} + \frac{13\sqrt{2}}{480} & \frac{1}{15} - \frac{13\sqrt{2}}{480} \end{array} \quad (\text{A.5})$$

Here, $c_2 = \frac{3-\sqrt{2}}{7}$, $c_3 = \frac{3+\sqrt{2}}{7}$ and $a_{32} = \frac{122+71\sqrt{2}}{7203}$.

A.3. SSP schemes from Gottlieb and co-workers [21]

$$\text{SSP-I2DRK3-2s:} \begin{array}{c|ccc|cc} 0 & 0 & 0 & -\frac{1}{6} & 0 \\ 1 & 0 & 1 & -\frac{1}{6} & -\frac{1}{3} \\ \hline & 0 & 1 & -\frac{1}{6} & -\frac{1}{3} \end{array} \quad (\text{A.6})$$

The coefficients for SSP-I2DRK4-5s are not as nice as for the above examples; we refer the reader to [21, Section 2.3, Paragraph "Fourth order"].

A.4. Some collocation-based Hermite-Birkhoff Runge-Kutta schemes

One set of coefficients is given in Table 2. The coefficients of the other collocation-based Hermite-Birkhoff Runge-Kutta schemes used in this work can be generated by the MATLAB code contained in our reproducibility repository [55].

Table 2: Runge-Kutta table of the continuous HB-I2DRK6-3s method. The method is uniformly sixth-order in $0 \leq \theta \leq 1$. As usual, the original Runge-Kutta method is obtained by setting $\theta = 1$. Note that the Butcher tableau corresponding to the second derivative has been printed under the one for the first derivative.

0	0	0	0
1/2	101/480	8/30	55/2400
1	7/30	16/30	7/30
	$4\theta^6 - \frac{68\theta^5}{5} + \frac{33\theta^4}{2} - \frac{23\theta^3}{3} + \theta$	$\frac{8\theta^3(6\theta^2-15\theta+10)}{15}$	$-\frac{\theta^3(120\theta^3-312\theta^2+255\theta-70)}{30}$
	0	0	0
	65/4800	-25/600	-25/8000
	5/300	0	-5/300
	$\frac{\theta^2(40\theta^4-144\theta^3+195\theta^2-120\theta+30)}{60}$	$\frac{8\theta^3(\theta-1)^3}{3}$	$\frac{\theta^3(40\theta^3-96\theta^2+75\theta-20)}{60}$